Chinese Chemical Letters 37 (2026) 110071

Contents lists available at ScienceDirect

Chinese Chemical Letters

journal homepage: www.elsevier.com/locate/cclet

Regulation of cancer cell apoptosis with DNA nanocalculator

Yongjian Jiang[a], Feng Cheng[a], Jun Zhou[b], Lei Zhan[a], Chunmei Li[a,*], Chengzhi Huang[a,*]

[a] Key Laboratory of Biomedical Analytics (Southwest University), Chongqing Science and Technology Bureau, College of Pharmaceutical Sciences, Southwest University, Chongqing 400715, China
[b] College of Computer and Information Science, Southwest University, Chongqing 400715, China

ARTICLE INFO

Article history:
Received 31 January 2024
Revised 6 May 2024
Accepted 30 May 2024
Available online 31 May 2024

Keywords:
Apoptosis
DNA nanocalculator
Logic gate
Nucleolin
Cytochrome c

ABSTRACT

Regulation of apoptosis represents a key parameter in all living organisms. In this paper, an input-induced logic-gated modular nanocalculator is designed to regulate cancer cell apoptosis by programmatically combining and connecting logic gate modules with different functions. *Via* rational design of the various logic gate modules of the nanocalculator, different apoptosis related operations including cancer cell targeting, apoptosis induction, and apoptosis monitoring could be performed. Importantly, each of these logic gate modules could independently perform apoptosis related YES logic operations when ran separately. After combining each YES logic gate module into a logic circuit and connecting it to the GO scaffold to construct a logic-gated nanocalculator, the input-induced logic-gated modular nanocalculator could selectively enter cancer cells and control the drug release to logically apoptosis (output), by performing AND logic gate operations when inputs (nucleolin and H^+) were included at the same time. Moreover, evidence suggests that these efficient logical calculations proceed in cancer cell apoptosis regulation without the general limiations of lithography in nanotechnology. As such, this work provides a new vision for the construction of a logic-gated modular nanocalculator with logical calculation proficiency potentially useful in cancer therapy and the regulation of life.

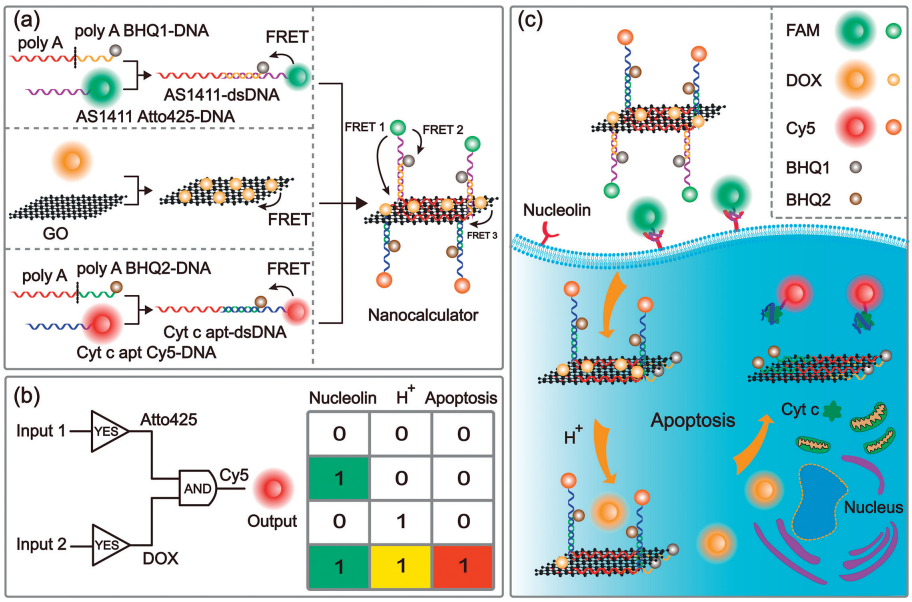
© 2025 Published by Elsevier B.V. on behalf of Chinese Chemical Society and Institute of Materia Medica, Chinese Academy of Medical Sciences.

Apoptosis describes the programmed cell death caused by changing environmental conditions or damages intended to maintain the stability of the intracellular environment [1–3]. A series of studies indicate that apoptosis is closely related to cancer and various drugs can play a therapeutic role by inducing apoptosis [4,5]. Therefore, the intelligent regulation of cell apoptosis is of great significance for the in-depth study of various cancer treatments. To date, significant progress has been made in cancer cell apoptosis-related research, including nanoprobes with apoptosis-inducing or apoptosis monitoring effects widely used in cancer cell treatments based on apoptosis [6–8]. However, severe problems still exist and limit an efficient apoptosis regulation. These include a general lack or low targeting ability of nanoprobes often not beneficial to achieve specific apoptosis desired to treat cancer [9,10]. More importantly, these nanoprobes when used for apoptosis monitoring often require the administration of secondary drugs to induce apoptosis [11,12]. In addition, due to the complexity of the apoptosis process and the diversity of biomarkers, highly efficient nanotechnologies are generally required for integrating multi parameter sensing, intelligent diagnosis, apoptosis induction, and apoptosis monitoring for effective apoptosis regulation.

So-called calculators may achieve information processing and signal transmission through the logical relationship between the input and output signals of logic gates [13]. In addition, biocomputing can provide intelligent solutions for complex biosensing projects, with great potential in multi-parameter sensing, intelligent diagnosis, and cancer treatment [14]. Based on this, we considered whether it may be possible to manufacture a biological "nanocalculator" that could control the delivery into cancer cells with subsequent drug release to regulate cancer cell apoptosis by executing logic gate operations. For the nanocalculator, logic gate circuit, the basis of logical judgement and data processing may enable the nanocalculator to perform complex logical functions through the combination and operation of logic gates [15–18]. Growing versatile biomolecules-based logic gate circuits composed of logic gates have been developed for multiple objectives that traditional silicon-dependant circuits may not be able to achieve [19–21]. In particular, as one of the critical biomacromolecules, DNA has been recognized as a superior candidate to program a DNA logic gate circuit without the confinement of lithography in nanotechnology due to its nanoscale dimensions, sequence programmability, and unique physicochemical properties [22–26]. By

* Corresponding authors.
E-mail addresses: licm1024@swu.edu.cn (C. Li), chengzhi@swu.edu.cn (C. Huang).

https://doi.org/10.1016/j.cclet.2024.110071
1001-8417/© 2025 Published by Elsevier B.V. on behalf of Chinese Chemical Society and Institute of Materia Medica, Chinese Academy of Medical Sciences.



Scheme 1. Schematic illustration of the input-induced logic-gated modular nanocalculator for cancer cell apoptosis regulation. (a) Assembly of the logic-gated modular nanocalculator. (b) Symbol and truth table of AND logic-gated modular nanocalculator. (c) Process of logical operation related to cancer cell apoptosis regulation using the input-induced logic-gated modular nanocalculator.

rational design of DNA sequence computing elements, a DNA-based logic gate circuit could be endowed with different functions [27–29]. Therefore, with guidance of a DNA-based logic gate circuit, the design of a logic-gated modular nanocalculator by programmatically combining and connecting logic gate circuit modules with different functions for logical integration of cancer cell apoptosis regulation was indeed possible as described below.

Motivated by these considerations, described herein is the rational design of an input-induced programmable logic-gated modular nanocalculator for logically integrating cancer cell targeting, apoptosis induction, and apoptosis evaluation functions based on combination and operation of logic gates for apoptosis regulation (Scheme 1). Due to the complexity of apoptosis and the suitable programmability of the logic-gated modular nanocalculator, logic gate modules that perform YES logic operations were programmed and systematically studied. Each of these logic gate modules of the nanocalculator could perform apoptosis-related YES logic operations individually when ran separately. After combining the logic gate modules into a logic circuit and connecting it to the GO scaffold to construct a logic-gated modular nanocalculator, the latter could selectively induce cancer cell apoptosis (output) by performing an AND operation when inputs (nucleolin and H^+) were provided at the same time, enabling a logical apoptosis regulation based on input induction through the logical integration of cancer cell targeting, apoptosis induction and evaluation.

Logic gates are the foundation of all calculators, and complex logic circuits in calculators may be composed of logic gates to perform corresponding logical operations. Due to the high programmability and ease of assembly of nanocalculators, logic gate modules that perform YES logic operations were programmed and systematically studied first. Utilizing the programmable nature of bases, a logic gate modular version of a cancer cell targeting unit was first designed that could be easily adapted to the use of DNA as recognition computing elements. Meanwhile, with the advantage of large specific surface area, GO themselves could efficiently co-assemble with of ssDNA for co-delivery, representing a suitable scaffold for the preparation of logic-gated modular nanocalculator by loading a logic circuit composed of logic gates. Moreover, GO could act as a receptor of fluorescence resonance energy transfer (FRET) to effectively quench the fluorescence of fluorescent dyes [30]. As such, it could be used to prepare logic-gated modular nanocalculator based on energy transfer. However, binding forces between GO and ssDNA are sensitive to environment changes and previous studies have demonstrated that GO features strong adsorption on adenine [31–33]. Our group has previously developed a robust DNA/GO nanodevice by using poly adenine (poly A) containing DNA as a stable anchor on GO. To further improve the anti-interference capability, GO and BHQ were simultaneously used as acceptors to minimized the false positive signal due to possible poly A DNA non-specific desorption.

Nucleolin is one of the most important tumor vessel markers in the field of cancer research. The main responsibility of nucleolin is the shuttling protein between cytoplasm and nucleus [34,35]. Some studies have revealed that nucleolin aptamer AS1411 could specifically bind to nucleolin, a feature that may be utilized to program a cancer cell targeting module [36]. Therefore, the cancer cell targeting module (Module 1) which could perform a YES logic gate operation was fabricated by immobilizing AS1411-dsDNA formed by hybridization of Atto425 modified AS1411 and poly A BHQ1-DNA onto the GO surface *via* poly A (Fig. 1a). The module was designed so that in the presence of the input (nucleolin) which selectively expressed on the surface of cancer cell membranes, Atto425-labeled AS1411 would be released from the scaffold due to specific binding of nucleolin and AS1411. The output of the Module 1 was the green fluorescence recovery of Atto425 (Fig. 1b). Fig. 1c shows the symbol and the truth table of the YES logic cancer cell targeting module. After hybridization of AS1411 Atto425-DNA with poly A BHQ1-DNA, the fluorescence of Atto425 decreased due to FRET between Atto425 and BHQ1 (Fig. 1d). When AS1411-dsDNA was adsorbed to GO by poly A, the fluorescence of Atto425 further decreased gradually upon increasing GO concentration, further confirming that dsDNA could be adsorbed on the GO scaffold through poly A (Fig. 1e).

The experimental results demonstrated that the Module 1 exhibited adequate biocompatibility (Fig. S1 in Supporting information). Furthermore, we applied Module 1 to the specific imaging of nucleolin on the surface of cancer cells to investigate whether the cancer cell targeting module could independently perform the

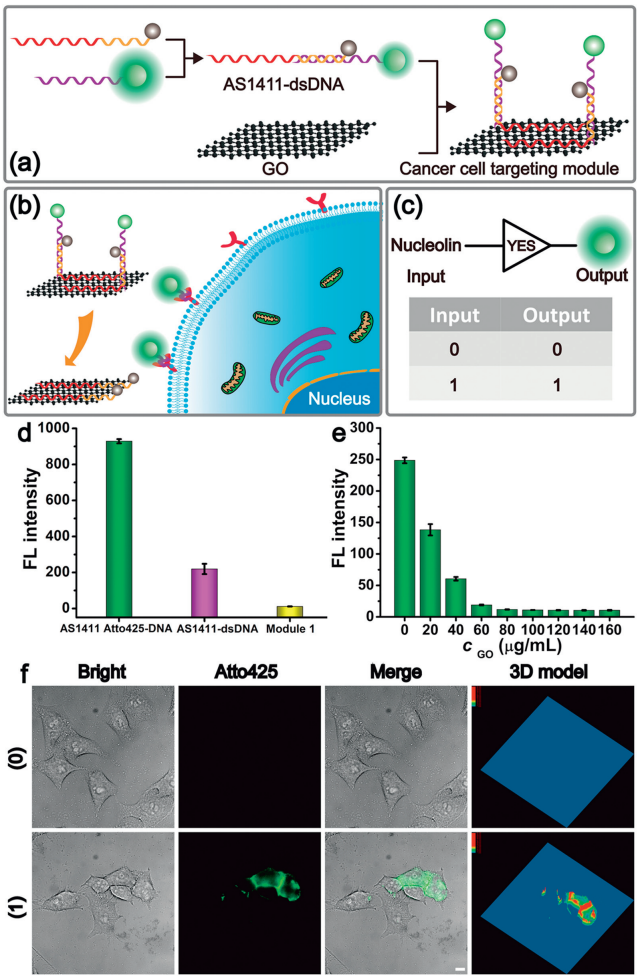


Fig. 1. The cancer cell targeting module performs the YES logic gate operation. (a) Principle of Module 1. (b) Principle of the Module 1 targeting nucleolin on the MCF-7 cell membrane. (c) The symbol and truth table of YES logic Module 1. (d) Fluorescence intensity of AS1411 Atto425-DNA, AS1411-dsDNA and Module 1. Concentrations: GO, 80 μg/mL; AS1411 Atto425-DNA, 200 nmol/L; AS1411-dsDNA, 200 nmol/L. (e) Fluorescence responses of AS1411-dsDNA (200 nmol/L) to GO of varying concentrations. (f) Confocal fluorescence imaging of MCF-7 cells incubated with YES logic Module 1 (5 μg/mL) at 4 °C for 30 min. Scale bars: 10 μm. (0) pre-incubation with AS1411; (1) without pre-incubation with AS1411.

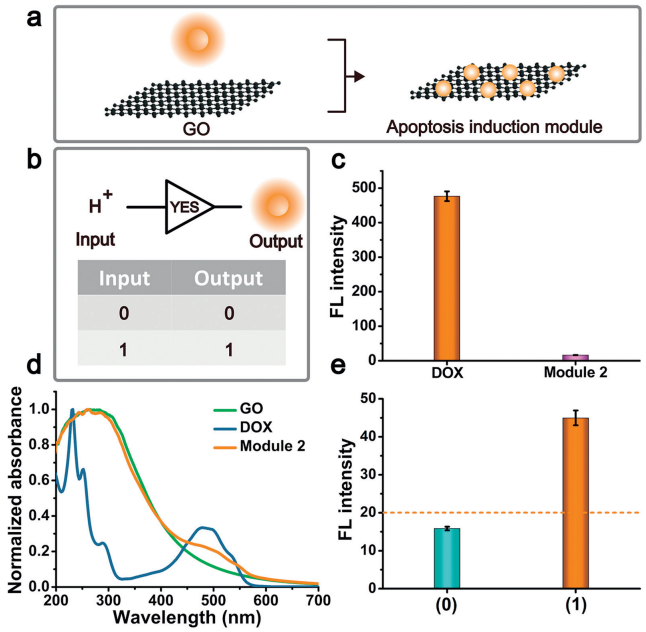


Fig. 2. The apoptosis induction module performs the YES logic gate operation. (a) Principle of Module 2. (b) The symbol and truth table of YES logic Module 2. (c) Fluorescence intensity of DOX and Module 2. Concentration: DOX, 10 μg/mL; GO, 100 μg/mL. (d) UV-vis spectra of DOX, GO and Module 2. (e) Computing result of YES logic Module 2 at different pH. (0) pH 7.4; (1) pH 5.5. Concentration: Module 2, 100 μg/mL. The orange dot line was set as the threshold value to judge the true (output = 1) and false (output = 0) output signals.

YES logic operation related to cancer cell targeting when ran separately (Fig. 1f). Both MCF-7 cells with or without pretreated by AS1411 to block nucleolins on the cell surface were subsequently incubated with Module 1, respectively. The detection of green fluorescence (Output) on the surface of unblocked MCF-7 cells demonstrated that Module 1 could selectively bind to nucleolins on the cell membrane. In contrast, no green fluorescence was observed on the surface of blocked cells, which proved that Module 1 could effectively recognize and bind nucleolins on the cell membrane by performing a YES logic gate operation. Moreover, compared with L02 cells, the green fluorescence of the Module 1 recovered on the surface of MCF-7 cells and A549 cells with high nucleolin expression indicated that the Module 1 could selectively target cancer cells (Fig. S2 in Supporting information).

As an anticancer agent that exerts therapeutic effects by inducing apoptosis, DOX was selected as a model apoptosis-inducing drug to aid the apoptosis-inducing module (Module 2) to perform a YES operation [37,38]. For Module 2, DOX was loaded onto GO *via* π-π stacking, hydrophobic, and hydrogen-bond interactions (Fig. 2a). DOX could be released from the GO surface under acidic conditions, resulting in the recovery of DOX fluorescence and a YES logic gate operation [39]. Fig. 2b shows the symbol and the truth table of the YES logic Module 2. After DOX was loaded on GO, the fluorescence of DOX was effectively quenched by GO (Fig. 2c). The peaks between 1100 cm^{-1} and 1500 cm^{-1} in the FTIR spectrum of DOX-GO indicated that DOX was successfully loaded on GO (Fig. S3 in Supporting information). The size increased from 185.3 ± 10.0 nm to 216.6 ± 7.4 nm upon DOX loading as evidenced by changes in dynamic light scattering (DLS) as shown in Fig. S4 (Supporting information). The UV-visible absorption spectra of DOX-GO showed an absorption peak at 484 nm corresponding to the presence of DOX, providing further evidence that DOX was successfully loaded onto the GO surface (Fig. 2d). The loading capacity of DOX assembled on GO was determined by fluorescence spectra, which was calculated by the difference between the original DOX concentration and the concentration of DOX in the supernatant. The linear regression equation (c, μg/mL) was $F = 74.5c_{DOX} + 1.03$ (correlation coefficient, $R^2 = 0.997$). After calculation, the loading capacity of DOX reached 99.9 μg/mg (Fig. S5 in Supporting information). The presence or absence of output signals were defined as 1 and 0, respectively. Meanwhile, it was defined as 1 only when the fluorescence intensity output by Module 2 was greater than the threshold, otherwise it was 0. With pH value decreased from 7.4 to 5.5, DOX loaded on Module 2 was released, and the output of module 2 at the set threshold was 1, which proved that Module 2 with input of H^+ could independently perform a YES logic operation related to the release of apoptosis-inducing drugs when ran separately (Fig. 2e).

Due to the programmable nature of the DNA-based systems, the construction of an apoptosis monitoring module is similar to that of a cancer cell targeting module (Module 3). Noteworthy in this context is the fact that cytochrome c (Cyt c) represents an important biomarker for early stage apoptosis [40,41]. Therefore, the apoptotic process could be monitored in real time by monitoring the change of Cyt c to evaluate the apoptosis-inducing effect of DOX. Initially, Cy5 modified Cyt c aptamer was hybridized with

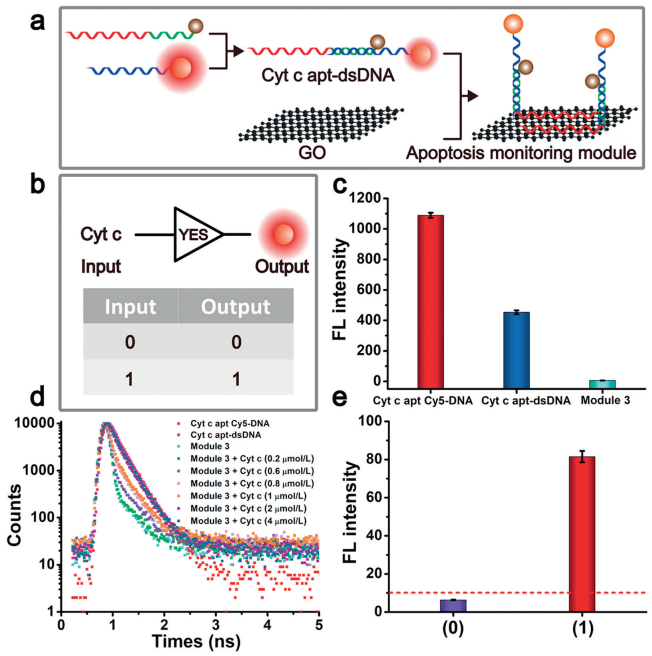


Fig. 3. The apoptosis monitoring module performs the YES logic gate operation. (a) Principle of Module 3. (b) The symbol and truth table of YES logic Module 3. (c) Fluorescence intensity of Cyt c apt Cy5-DNA, Cyt c apt-dsDNA and the Module 3. Concentrations: GO, 110 μg/mL; Cyt c apt Cy5-DNA, 200 nmol/L; Cyt c apt-dsDNA, 200 nmol/L. (d) Fluorescence lifetime measurements of Cy5 in the absence and presence of BHQ2, GO, and difference concentrations of Cyt c. (e) Computing result of YES logic Module 3 in the presence and absence of 0.8 μmol/L Cyt c input. (0) in the absence of Cyt c; (1) in the presence of Cyt c. The red dot line was set as the threshold value to judge the true (output = 1) and false (output = 0) output signals.

partially complementary poly A BHQ2-DNA to form dsDNA (Cyt c apt-dsDNA), which was then loaded onto GO by poly A to assemble Module 3 (Fig. 3a). In the presence of Cyt c (Input), the hybridized duplexes of Module 3 dissociated, preventing Cyt c apt Cy5-DNA from binding to GO and poly A BHQ2-DNA and resulting in fluorescence recovery of Cy5 (Output) with a YES logic gate operation. Fig. 3b shows the symbol and the truth table of the YES logic dissociation. After hybridization of Cyt c apt Cy5-DNA with poly A BHQ2-DNA, the fluorescence of Cy5 decreased and when Cyt c apt-dsDNA was adsorbed to GO by poly A, the fluorescence of Cy5 decreased even further (Fig. 3c). The fluorescence intensity of Cyt c apt-dsDNA was found to decrease upon increasing the GO concentration (Fig. S6 in Supporting information) and the fluorescence lifetime of the Cy5 donor was shortened to 0.407 ns after noncovalent assembly of Cyt c Apt-dsDNA on the GO scaffold *via* poly A extension. It subsequently recovered to 0.440, 0.623, 0.100, 1.14, 1.76 and 1.86 ns upon addition of different Cyt c concentrations, respectively (Fig. 3d).

Next, we focused on Module 3 optimization and debugging to improve analytical performance. Influences of varying base numbers in the toehold domain and the concentrations of GO were explored. The F/F_0 value was the largest when the toehold domain was 14 (Figs. S7a and b in Supporting information). The F/F_0 value increased gradually with increasing GO concentration, and reached a maximum at 110 μg/mL (Figs. S7c and d in Supporting information). This was due to the concentration of GO that was too high for Cyt c apt Cy5-DNA to release from GO. Therefore, the signal noise was relatively low. After debugging Module 3, Cyt c as an input was incubated together with Module 3 and the output of module 3 at the set threshold was 1, which proved that it could independently perform YES logic operations related to apoptosis monitoring (Fig. 3e). Furthermore, concentration row experiments of the YES logic Module 3 were conducted (Fig. S8 in Supporting information). The fluorescence of Cy5 increased gradually after addition of various concentrations of Cyt c and the YES logic Module 3 could differentiate between 0.05 μmol/L and 1 μmol/L Cyt c. The limit of detection for the YES logic Module 3 was 0.042 μmol/L ($3\sigma/k$). More importantly, the fluorescence of Cy5 was restored only in the presence of Cyt c, which further demonstrated the feasibility of Module 3 to perform a YES logical operation on input Cyt c (Fig. S9 in Supporting information).

Subsequently, the nuclease stability of the Module 3 was investigated to ensure accurate apoptosis monitoring. The fluorescence readout of Module 3 had no obvious changes both in the absence and in the presence of enzyme deoxyribonuclease I (DNase I), indicating that the GO scaffold could effectively protect DNA from enzymatic cleavage in cells (Fig. S10 in Supporting information). In addition, to investigate the accuracy of Module 3 during operation, a control Module 3 was designed for comparison by directly assembling a Cy5 modified Cyt c aptamer onto GO. Compared to the control Module 3, Module 3 featured suitable stability in the RPMI culture medium (Fig. S11 in Supporting information). In order to determine the stability of apoptosis monitoring module in complex cellular environments, the apoptosis monitoring module and cancer cell targeting module were simultaneously loaded on the GO scaffold to construct Module 3-1. This Module 3-1 not only had the function of monitoring cell apoptosis, but also had the function of targeting cancer cells, making it easier to enter cancer cells. Similarly, based on the GO scaffold loaded cancer cell targeting module, Cyt c apt Cy5-DNA was directly adsorbed to prepare control Module 3-1 (Fig. S12a in Supporting information). Next, control Module 3-1 and Module 3 were incubated with MCF-7 cells separately in the absence of DOX. As a result, we found that red fluorescence of Cy5 in the control Module 3-1 was restored while the red channel of the Module 3-1 did not show any fluorescence, indicating that the stability of the module was improved through poly A and the one-donor-two-acceptor design (Fig. S12b in Supporting information).

Next, we sought to confirm the proof-of-principle of this logic-gated modular nanocalculator with apoptosis functional integration modules. By integrating diverse functional logic gate moieties like a cancer cell targeting module, an apoptosis induction module, and apoptosis monitoring module into one system to form a logic gate circuit, a logic-gated modular nanocalculator using GO as scaffold could be constructed to perform AND logic operations. For the logic-gated modular nanocalculator, Atto425 and Cy5 dyes were used, corresponding to the quencher of BHQ1 and BHQ2, respectively (Fig. 4a). Standardized Commission Internationale de l'Eclairage (CIE) calculations were used to quantify the chromaticity of Atto425, DOX and Cy5. By comparing the CIE coordinates of Atto425 (0.135, 0.322), DOX (0.528, 0.469) and Cy5 (0.731, 0.269), the changes in fluorescence signals of different colors caused by different modules could provide information on cancer cell targeting, apoptosis induction, and apoptosis monitoring, respectively (Fig. 4b). After immobilization of AS1411-dsDNA, DOX, and Cyt c apt-dsDNA on the surface of the GO scaffold *via* poly A, the fluorescence of Atto425, DOX, and Cy5 in the logic-gated modular nanocalculator was found to be further reduced (Fig. S13 in Supporting information). After DOX loading, the zeta potential of DOX-GO turned slightly more positive, which could be attributed to the positive charge of DOX. Subsequently, DOX-GO further loaded ds-DNA to prepare a logic-gated modular nanocalculator, resulting in the zeta potential being more negative due to the polyanionic nature of DNA (Fig. 4c). Atomic force microscopy (AFM) demonstrated that the thickness of GO increased from 0.76 ± 0.09 nm to 1.74 ± 0.27 nm after loading the DNA module units on the GO scaffold (Figs. 4d–f). The fluorescence of DOX in the logic-gated modular nanocalculator could be gradually recovered upon decreasing

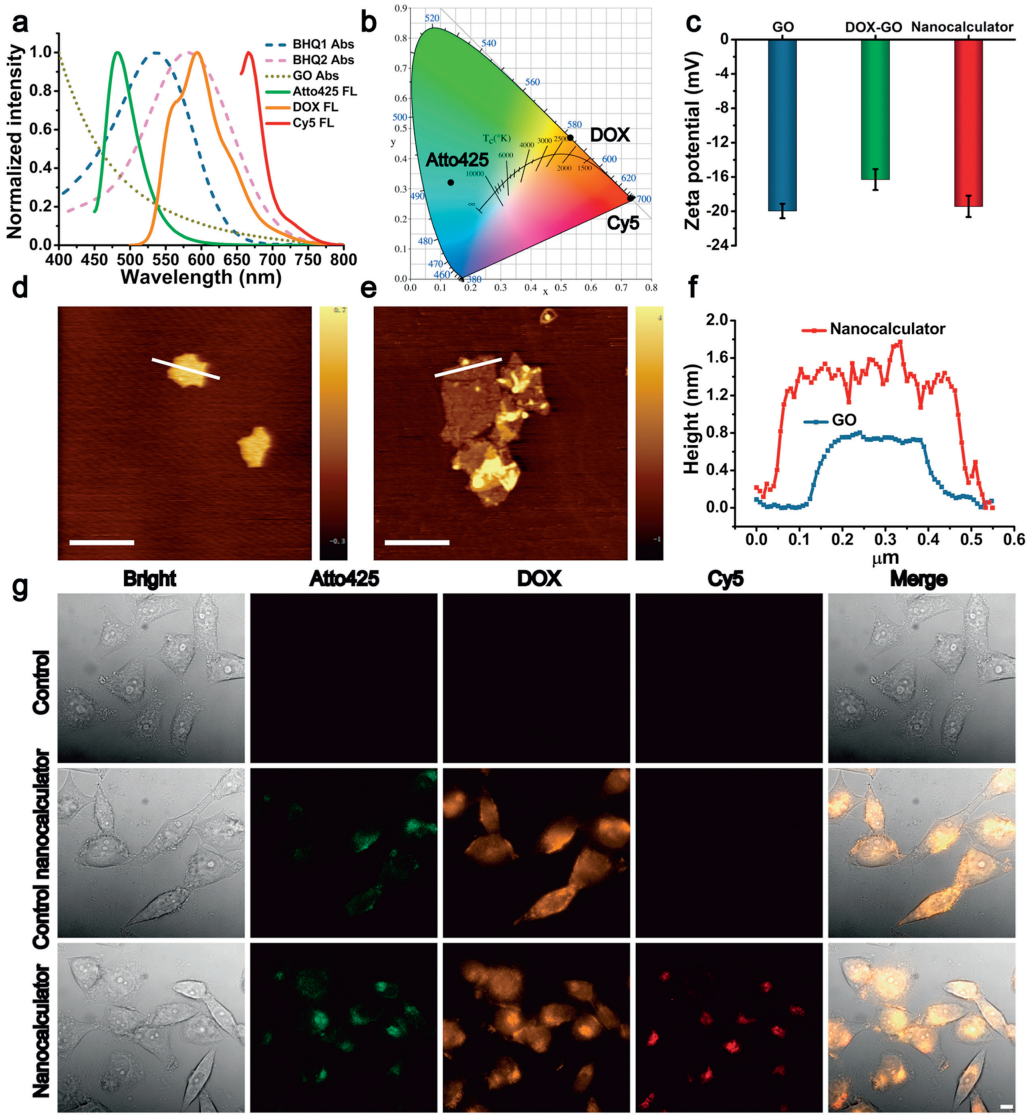


Fig. 4. Functional debugging of logic-gated modular nanocalculator with functional integration modules. (a) Normalized fluorescence spectra of Atto425, DOX and Cy5 and absorption spectra of BHQ-1, BHQ-2 and GO. Excitation wavelength: Atto425, 425 nm; DOX, 480 nm; Cy5, 649 nm. (b) The CIE 1931 chromaticity coordinates of Atto425, DOX and Cy5. (c) Zeta potential of GO, DOX-GO and logic-gated modular nanocalculator. AFM images of GO (d) and the logic-gated modular nanocalculator (e). Scale bars: 0.5 μm. (f) The height profiles along the white line in panels of GO and the logic-gated modular nanocalculator, respectively. (g) Confocal fluorescence images of MCF-7 cells before (Control) and after incubation with the control nanocalculator (5 μg/mL) and logic-gated modular nanocalculator (5 μg/mL) respectively. Scale bars: 10 μm.

the pH (Fig. S14a in Supporting information). Conversely, upon increasing the Cyt c concentration, the red fluorescence of the apoptosis monitoring module in the logic-gated modular nanocalculator gradually recovered (Fig. S14b in Supporting information), indicating that the logic-gated modular nanocalculator could perform AND logic gate operations.

Subsequently, the logical operation ability of each module in the logic-gated modular nanocalculator during cell imaging was explored. At first, the logic-gated modular nanocalculator was applied to the imaging of nucleolin on the surface of MCF-7 cells. The green fluorescence on the surface of MCF-7 cells demonstrated that the logic-gated modular nanocalculator could selectively bind to nucleolins on the cell membrane (Fig. S15 in Supporting information). By incubating the logic-gated modular nanocalculator with MCF-7 cells and MCF-7 cells with the nucleolus blocked by AS1411, the orange and red fluorescence of DOX and Cy5 channels in MCF-7 cells with nucleolus blocked by AS1411 did not recover, indicating the effectiveness of the Module 1 in the logic-gated modular nanocalculator for targeting cancer cells (Fig. S16 in Supporting information). In addition, a control nanocalculator was prepared for comparison by using a random sequence instead of the Cyt c aptamer in Module 3 of the logic-gated modular nanocalculator. After incubating the control nanocalculator with MCF-7 cells, it was found that no recovery of red fluorescence took place, indicating that red fluorescence was caused by the specific binding of Cyt c with its aptamer in Module 3 resulting in the release of the aptamer from the surface of GO (Fig. 4g).

After this proof-of-principle demonstration of the programmability of this logic-gated modular nanocalculator, we sought to expand this application to programmable apoptosis regulation. When nucleolin and H^+ were input simultaneously, the nanocalculator could perform an AND logic gate operation resulting in apoptosis signal output represented by Cy5 fluorescence (Fig. 5a). Fig. 5b shows the symbol and the truth table of the AND logic-gated modular nanocalculator. To test whether the logic-gated modular nanocalculator could achieve apoptosis regulation by performing an AND logic gate operation, the following experiment was carried out: MCF-7 cells were pretreated with AS1411 to block nu-

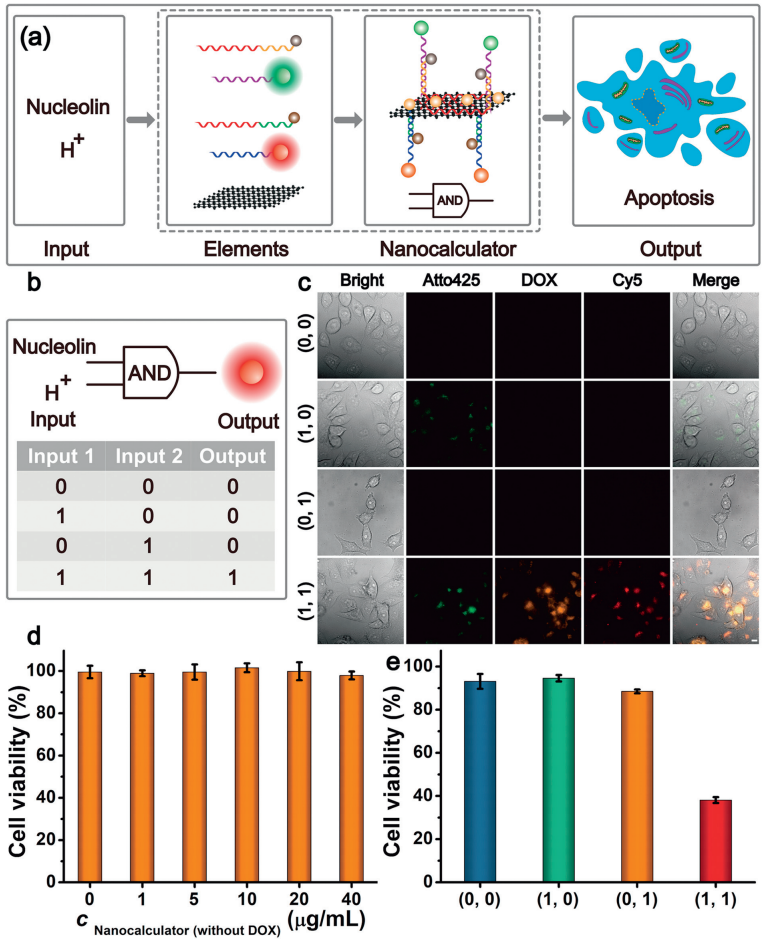


Fig. 5. The logic-gated modular nanocalculator performs the AND logic gate operation. (a) Schematic diagram of the logic-gated modular nanocalculator regulating apoptosis by performing AND logic gate operation. (b) The truth table of AND logic-gated modular nanocalculator. (c) Confocal imaging of logic-gated modular nanocalculator (5 μg/mL) performing AND logic gate. Scale bars: 10 μm. (d) Cell viability of MCF-7 cells (100 μL, 1×10^5 /mL) after incubated with different concentrations of the logic-gated modular nanocalculator without module 2 assembly. (e) Cytotoxicity of the logic-gated modular nanocalculator (5 μg/mL) performing AND logic gate.

cleolins on the MCF-7 cells surface, followed by treatment with our logic-gated modular nanocalculator. Furthermore, MCF-7 cells were pretreated with chloroquine to increase the pH of the cells, followed by treatment with the logic-gated modular nanocalculator. Meanwhile, MCF-7 cells were pretreated by AS1411 and chloroquine at the same time, followed by treatment with this logic-gated modular nanocalculator. MCF-7 cells subjected to treatment with the above three methods showed no obvious red fluorescence signal. In contrast, once the two inputs (*i.e.*, nucleolin and low pH) of the AND logic gate were fulfilled, fluorescence of Cy5 represented as output signal could be detected, further indicating that the logic-gated modular nanocalculator could target cancer cells, induce apoptosis of cancer cells and evaluate apoptosis through AND logic gate operations (Fig. 5c). In addition, the AND logic operation of the logic-gated modular nanocalculator could also be confirmed by cytotoxicity experiments. If DOX was not loaded on the logic-gated modular nanocalculator, the nanocalculator featured good biocompatibility (Fig. 5d). Only if two inputs (nucleolin and low pH) of the AND logic gate were fulfilled simultaneously, the nanocalculators exhibited high cytotoxicity, demonstrating that the logic-gated modular nanocalculator could perform AND logic operations to achieve apoptosis regulation (Fig. 5e).

Furthermore, in order to verify whether the logic-gated modular nanocalculator could be used to achieve programmed functional integration, the nanocalculator was incubated with MCF-7 cells to induce apoptosis. As shown in Fig. S17 (Supporting information), green fluorescence appeared first in MCF-7 cells, indicating that the logic-gated modular nanocalculator could selectively and accurately target cancer cells *via* a cancer cell targeting module. After the nanocalculator entered MCF-7 cells, DOX was desorbed from the GO, and orange fluorescence stemming from DOX was recovered, allowing for real-time monitoring of drug release. In the early stages of apoptosis, Cyt c is released from the mitochondria into the cytoplasm. Therefore, with progression of DOX-induced apoptosis, the red fluorescence of the nanocalculators gradually recovered upon increasing the incubation time, indicating that cancer cell targeting, apoptosis induction and apoptosis evaluation could successfully be integrated.

In this work, an input-induced logic-gated modular nanocalculator was constructed by combining YES logic gate modules with cancer cell targeting, apoptosis induction, and apoptosis monitoring functions into one logic circuit and connecting it to a GO scaffold. Each of these three logic gate modules could perform an apoptosis-related YES logic gate operation individually when ran in a separate fashion. Furthermore, taking advantage of the logical relationship between the input and output of the logic gate circuit, the logic-gated modular nanocalculator could selectively enter cancer cells and control drug release to logically regulate events like apoptosis (output) by performing an AND logic operation through recognition of different inputs (nucleolin and H^+). The success-

ful operation of this logic-gated modular nanocalculator, which is not limited by nanotechnology lithography processes, in cancer cell apoptosis regulation may ultimately offer a new therapeutic approach to treat cancer or regulate other cellular activities.

Declaration of competing interest

The authors declare that they have no known competing financial interests or personal relationships that could have appeared to influence the work reported in this paper.

CRediT authorship contribution statement

Yongjian Jiang: Conceptualization, Data curation, Formal analysis, Funding acquisition, Investigation, Methodology, Writing – original draft, Software, Visualization. **Feng Cheng:** Software, Investigation. **Jun Zhou:** Conceptualization, Software. **Lei Zhan:** Conceptualization, Software. **Chunmei Li:** Conceptualization, Funding acquisition, Supervision, Visualization, Writing – review & editing, Project administration, Validation. **Chengzhi Huang:** Funding acquisition, Project administration, Resources, Writing – review & editing, Conceptualization, Supervision.

Acknowledgments

This work was financially supported by the National Natural Science Foundation of China (NSFC, Nos. 22134005 and 22074124), Chongqing Talents Program for Outstanding Scientists (No. cstc2021ycjh-bgzxm0178), Natural Science Foundation of Chongqing (No. CSTB2022NSCQ-MSX0521) and the Chongqing Graduate Student Scientific Research Innovation Project (No. CYB21119). The authors thank Yanjie Li, College of Pharmaceutical Sciences, Southwest University, for helping to acquire AFM data.

Supplementary materials

Supplementary material associated with this article can be found, in the online version, at doi:10.1016/j.cclet.2024.110071.

References

[1] M. Sun, C.Y. Wang, M.C. Lv, et al., J. Am. Chem. Soc. 144 (2022) 7337–7345.
[2] S. Victorelli, H. Salmonowicz, J. Chapman, et al., Nature 622 (2023) 627–636.
[3] R.S. Li, J.H. Liu, H. Shi, et al., Nano Lett. 21 (2021) 8455–8465.
[4] C. Xing, Q.T. Lin, Y.T. Chen, et al., Acta Biomater. 167 (2023) 564–573.
[5] J.C. Tang, W.C. Li, T.Y. Chiu, et al., Nature 622 (2023) 507–513.
[6] H.R. Lin, Y.J. Jiang, F. Cheng, et al., ACS Appl. Nano Mater. 4 (2021) 13469–13476.
[7] D.W. Hwang, H.Y. Kim, F.Y. Li, et al., Biomaterials 121 (2017) 144–154.
[8] P.L. Chen, P.Y. Huang, J.Y. Chen, et al., Biomaterials 286 (2022) 121593.
[9] X.X. Shi, H.M. Meng, X. Geng, et al., ACS Sens. 5 (2020) 3150–3157.
[10] J.R. Tang, C.X. Huang, J.Y. Shu, et al., Anal. Chem. 90 (2018) 5865–5872.
[11] J.H. Choi, J.W. Choi, Nano Lett. 20 (2020) 7100–7107.
[12] T.T. Chen, X. Tian, C.L.W. Liu, et al., J. Am. Chem. Soc. 137 (2015) 982–989.
[13] R. Liu, Y.M. Han, F. Sun, et al., Adv. Mater. 34 (2022) 2202135.
[14] D. Hartmann, R. Chowdhry, J.M. Smith, et al., J. Am. Chem. Soc. 145 (2023) 9471–9480.
[15] W.Y. Lv, C.H. Li, F.F. Yang, et al., Angew. Chem. Int. Ed. 61 (2022) e202115561.
[16] H.D. Huang, Z.Z. Guo, C.J. Zhang, et al., ACS Appl. Mater. Interfaces 13 (2021) 30397–30403.
[17] X.D. Yang, J. Li, R. Song, et al., Nat. Nanotechnol. 18 (2023) 471–478.
[18] H. Liu, Z.H. Ming, Y.P. Zhang, et al., Chin. Chem. Lett. 35 (2024) 108555.
[19] E. Chatir, A. Khettabi, F. Lafolet, et al., Chem. Mater. 34 (2022) 5912–5918.
[20] Z. Guo, O. Smutok, C.E. Ayva, et al., Nat. Nanotechnol. 18 (2023) 1327–1334.
[21] Z.F. Gu, A.C. Fu, R. Qiu, et al., Chin. Chem. Lett. 33 (2022) 2711–2714.
[22] E. Del Grosso, P. Irmisch, S. Gentile, et al., Angew. Chem. Int. Ed. 61 (2022) e202201929.
[23] X.W. Yan, H.Q. Zhang, Z.X. Wang, et al., Chem. Commun. 54 (2018) 7491–7494.
[24] J.L. Wang, J. Li, Y. Chen, et al., Nano Lett. 22 (2022) 8216–8223.
[25] W.K. Zhong, L. Huang, Y.H. Lin, et al., Sci. China Mater. 66 (2023) 2938–2946.
[26] S. Jiang, Y.B. Cai, Q.Y. Zhang, et al., Nano Lett. 23 (2023) 10625–10632.
[27] Y.C. Guo, J.T. Ren, E.K. Wang, Nano Today 44 (2022) 101476.
[28] D. Wang, S.H. Li, Z.L. Zhao, et al., Angew. Chem. Int. Ed. 60 (2021) 15816–15820.
[29] J.K. Jung, C.M. Archuleta, K.K. Alam, et al., Nat. Chem. Biol. 18 (2022) 385–393.
[30] Y. Zhang, Y. Liu, S.J. Zhen, et al., Chem. Commun. 47 (2011) 11718–11720.
[31] X.H. Tan, T. Chen, X.L. Xiong, et al., Anal. Chem. 84 (2012) 8622–8627.
[32] J.W. Liu, Phys. Chem. Chem. Phys. 14 (2012) 10485–10496.
[33] Y.J. Jiang, N. Wang, F. Cheng, et al., Anal. Chem. 92 (2020) 11565–11572.
[34] S.P. Li, Q. Jiang, S.L. Liu, et al., Nat. Biotechnol. 36 (2018) 258–264.
[35] S.X. Zhang, C. Chen, C. Xue, et al., Angew. Chem. Int. Ed. 59 (2020) 14584–14592.
[36] C.H. Li, W.Y. Lv, F.F. Yang, et al., ACS Appl. Mater. Interfaces 14 (2022) 12059–12067.
[37] J.Y. Zhang, F.M. Chen, Y.X. Li, et al., Nano Today 53 (2023) 102039.
[38] C. Xue, S.B. Zhang, X. Yu, et al., Angew. Chem. Int. Ed. 59 (2020) 17540–17547.
[39] T.J. Yin, J.Y. Liu, Z.K. Zhao, et al., Adv. Funct. Mater. 27 (2017) 1604620.
[40] X.L. Zhang, N.S. Liao, G. Chen, et al., Nanoscale 9 (2017) 10861–10868.
[41] H. Choi, G. Park, E. Shin, et al., Chem. Sci. 13 (2022) 6197–6204.